University of São Paulo
São Carlos Institute of Physics

Author: Lucas Bins Ely Tsunaki

Quantum Information Processing with Nitrogen Vacancy Centers in Diamonds

Advisor: Prof. Dr. Sérgio Ricardo Muniz

Course completion assignment project presented to the Undergraduate Program at the São Carlos Institute of Physics, University of São Paulo, to the degree of Bachelor of Physics, Major in Theoretical and Experimental.

São Carlos, SP
July 2020

Abstract

A major challenge in the physical realization of quantum computing resides in characterizing a platform and developing the necessary techniques to produce any quantum algorithm or protocol with fidelity. Distinguishing itself among such platforms, the nitrogen vacancy center in diamonds is a substitutional point defect which occurs in the carbon lattice. The focus of this study is then to analyze the system as a two qubit quantum processor and the corresponding techniques required for the initialization, manipulation and reading of its quantum states. Firstly, we review the principles of quantum information processing with an ensemble of two energy level spins. The system's properties and a simplified model Hamiltonian are then analyzed, alongside its energy structure. Based on that, we discuss how the quantum states can be initialized and measured by a combination of optical and magnetic resonance techniques, while quantum gates can be achieved by the composition of microwave pulses. As an illustration of the studied concepts, we conclude by discussing the implementation of a non-thermalizing quantum thermometer protocol using the nitrogen vacancy system.

Keywords: Nitrogen vacancy center in diamonds. Quantum information processing. Quantum thermometry.

1 Introduction

The past few years have seen substantial progress in the area of quantum computing. Experimental realizations were accomplished throughout different physical systems using a range of techniques. This crescent research in the area is attributed to the many applications that it could bring, for instance, related to quantum simulations in computational chemistry, or integer factorization in quantum cryptography. Another motivating factor is the potential of Quantum Advantage over classical computers in many specific tasks, where a quantum computer would realize them in exponentially shorter times. (1)

In contrast to classical computers, a quantum computer uses quantum properties to process information. The basic unit of quantum information is denominated qubit, short for quantum bit, which rather than being a binary system, can assume superposition of states and even be entangled with other qubits. These properties are the backbone of quantum computing which provides computational advantages over classical binary states.

Nevertheless, the physical realization of quantum computing faces several barriers, namely the loss of coherence of qubits due to unwanted external fluctuations, scalability and the development of the right techniques to manipulate and control qubits with fidelity. The challenge imposed by these barriers resides in finding appropriate physical

platforms that can avoid or minimize these problems. In this context, the nitrogen vacancy center (NV) has been focus of numerous research on the prospects of its use in quantum computing in recent years (2 - 5).

The NV center is a point defect in diamonds composed of a nitrogen atom adjacent to a vacancy in the carbon lattice. Besides applications as a nanosensor and in quantum metrology (6 - 7), the NV also presents itself as a promising platform for quantum computing due to its interesting properties. The center has well-defined quantum states within the band-gap, which can be easily initialized via an optical pumping mechanism and readout by the resulting fluorescence intensity. Furthermore, the spin states can be manipulated by magnetic resonance techniques and the rigid diamond lattice shields the center from thermal decoherence factors, resulting in relatively long coherence times even at room temperature.

In sight of such promise in the platform to deliver quantum information processing (QIP), this work is focused on the prospects of using the NV center for QIP and the development of the required techniques to implement it in the laboratory. We begin in section 2 by presenting the main principles of quantum information theory, followed by a discussion of quantum information processing with an ensemble of two energy level spins. In section 3, we examine the NV center main interactions and the correspondent energy structure, considering their practical relevance in the initialization, manipulation and reading of quantum states. Lastly, section 4 illustrates an interesting application of the concepts previously discussed, where we present a quantum protocol to use the NV center as a non-thermalizing quantum thermometer, which is currently being developed at the Quantum Technologies Laboratory at IFSC/USP.

2 Quantum Information Processing and Magnetic Resonance

This section lays some of the basic principles of QIP which are going to be employed later. Although the discussion is general and can be applied to other systems, it is motivated by the practical use with the NV center. In section 2.1, we introduce the general theoretical formalism of quantum information, independent of any physical implementation. In 2.2, we discuss QIP with an ensemble of individual quantum processors and present the density matrix formalism. Ultimately, section 2.3 depicts a spin-$\frac{1}{2}$ ensemble, where we analyze how its two energy levels can be used as a computational basis and how to manipulate their quantum states with magnetic resonance techniques.

2.1 Principles of Quantum Information

In classical computing, information is encoded in binary digits (bits) that assume values either 0 or 1. Classical bits can be physically represented by the absence or presence of electric current in a circuit. In contrast, qubits are expressed by quantum states in a physical system, where ordinarily two of the quantum states of the system are associated with a 2-dimensional computational basis: $\{|0\rangle, |1\rangle\}$. By doing so, a general state of a qubit is expressed by a linear combination of the basis states, which can be represented in matrix notation,

$$|\psi\rangle = \alpha\,|0\rangle + \beta\,|1\rangle \equiv \alpha \begin{bmatrix} 1 \\ 0 \end{bmatrix} + \beta \begin{bmatrix} 0 \\ 1 \end{bmatrix} = \begin{bmatrix} \alpha \\ \beta \end{bmatrix}, \tag{2.1}$$

where α and β are complex numbers and $|\alpha|^2 + |\beta|^2 = 1$, with $|\alpha|^2$ and $|\beta|^2$ being the probability of measuring the qubit in the states $|0\rangle$ and $|1\rangle$, respectively.

Apart from being able to encode information in qubits, it is also required that the information can be manipulated and controlled. To achieve this, we make use of quantum logic gates, which are unitary transformations on one or more qubits, resulting in an outcome. Quantum gates that act on one qubit can be represented by 2×2 matrices in this Hilbert space. As an illustration, a relevant gate in this work is the Z gate, defined as

$$Z\,|\psi\rangle \equiv \begin{bmatrix} 1 & 0 \\ 0 & -1 \end{bmatrix} \begin{bmatrix} \alpha \\ \beta \end{bmatrix} = \begin{bmatrix} \alpha \\ -\beta \end{bmatrix}. \tag{2.2}$$

Which acts on a qubit resulting in a phase shift of π on the second component. The Z gate can also be seen as a rotation of π around the z-axis, as we are going to discuss in section 2.3. Another relevant gate in QIP is the Hadamard, acting on one qubit creating superposition between the basis states and defined by

$$H\,|\psi\rangle \equiv \frac{1}{\sqrt{2}} \begin{bmatrix} 1 & 1 \\ 1 & -1 \end{bmatrix} \begin{bmatrix} \alpha \\ \beta \end{bmatrix} = \frac{1}{\sqrt{2}} \begin{bmatrix} \alpha + \beta \\ \alpha - \beta \end{bmatrix}. \tag{2.3}$$

Most quantum processors have more than one qubit. In this case, each qubit occupies a different computational subspace. For the purpose of mathematically describing the state of the set of qubits, a tensor product of the different subspaces is performed. Therefore, in a 2-qubit system, we have a 4-dimensional basis given by $\{|0\rangle, |1\rangle\} \otimes \{|0\rangle, |1\rangle\} \equiv \{|00\rangle, |01\rangle, |10\rangle, |11\rangle\}$.

To apply a quantum logic gate in this new space, it is required to specify which unitary transformation is being applied to which qubit, e.g., if we want to apply a Hadamard gate to the first qubit while the second remains constant, the gate is written as

$$(H_1 \otimes \mathbb{1}_2)\,|\psi_1\psi_2\rangle = (H_1\,|\psi_1\rangle) \otimes (\mathbb{1}_2\,|\psi_2\rangle) = (H_1\,|\psi_1\rangle) \otimes |\psi_2\rangle, \tag{2.4}$$

where $\mathbb{1}$ is the identity operator. Another relevant quantum gate for 2-qubits is the Controlled Z gate, defined by

$$CtrZ \equiv |0\rangle \langle 0|_1 \otimes \mathbb{1}_2 + |1\rangle \langle 1|_1 \otimes Z_2. \tag{2.5}$$

In this gate, if the first qubit is in the state $|0\rangle_1$, then the second qubit it is not altered, but if the first qubit is in the state $|1\rangle_1$, then the second qubit goes through a Z gate defined by Eq. (2.2).

2.2 Quantum Information Processing of Ensembles

Many quantum computers, particularly the one studied in this work, are composed of an ensemble of individual atomic scale quantum processors following the formalism developed in section 2.1. Collectively, they execute redundant parallel processing, in this case, without increasing the computational power of the system. It is not practical, nor necessary, to have knowledge over all quantum states of the ensemble, which makes advantageous to use statistical averages, where the macroscopic observables measured in laboratory are a result of the average of all quantum states.

The most appropriate approach to represent a mixed state ensemble is using the density matrix operator (8)

$$\rho \equiv \sum_n p_n |\psi_n\rangle \langle \psi_n| , \tag{2.6}$$

where $|\psi_n\rangle \langle \psi_n|$ is the outer product of the possible quantum states and p_n is the statistical probability of a constituent of the ensemble being in the $|\psi_n\rangle$ state. This operator is Hermitian and the diagonal elements of the matrix physically represent the populations of the quantum states, while the off-diagonal elements are called coherences and are related to superpositions between them. By construction $\mathrm{Tr}(\rho) = 1$.

Under thermal equilibrium at room temperature, a general ensemble will not present coherences and the probabilities p_n of the populations will be given simply by the Maxwell-Boltzmann distribution (9). With that, Eq. (2.6) can be represented in the computational basis as

$$\rho_0 = \frac{e^{-\mathcal{H}_0/kT}}{\mathcal{Z}} = \frac{1}{\mathcal{Z}} \begin{bmatrix} e^{-E_1/kT} & 0 & \cdots \\ 0 & e^{-E_2/kT} & \cdots \\ \vdots & \vdots & \ddots \end{bmatrix}, \tag{2.7}$$

with $\mathcal{H}_0$ being the system's Hamiltonian that lead to the thermal equilibrium, E_n its energy levels and $\mathcal{Z} = \sum_n^N e^{-E_n/kT}$ the Partition function. Using the representation of Eq. (2.7), it is practical to calculate the average value of some operator A, corresponding to some measurable observable,

$$\langle A \rangle = \mathrm{Tr}(\rho A). \tag{2.8}$$

It is also fundamental to study how the density matrix evolves with time under the interaction with some time indepent Hamiltonian $\mathcal{H}$. For that, the time evolution

operator is used (8):

$$\rho(t) = e^{-i\mathcal{H}t/\hbar}\ \rho(0)\ e^{i\mathcal{H}t/\hbar}. \tag{2.9}$$

With this, it is possible to predict the effect of some specific interaction on the populations and coherences, alongside designing sequences of pulses in order to reproduce some quantum gate, as it is going to be discussed in the next section.

2.3 Two Energy Level Spin Systems and Rotations

One of the main focuses of experimental research on quantum computing is to identify a physical platform and develop the required techniques that can produce the logic of QIP, briefly presented in section 2.1. In order to achieve such a system with two distinct quantum states $|0\rangle$ and $|1\rangle$, it is required a two energy level structure with a feasible mechanism to generate transitions between them. The spin-$\frac{1}{2}$ can constitute such a two energy level system and be manipulated by a wide range of magnetic resonance techniques for the purpose of being used as a quantum processor. As it shall become clear in section 3, the NV center can also be modeled by the formalism presented in this section, despite not being a spin-$\frac{1}{2}$ system.

Primarily, let us consider an ensemble of non-interacting spins-$\frac{1}{2}$ at temperature T. Their intrinsic magnetic moment is $\vec{\mu}_I = \gamma\hbar\vec{I}$, in case the spins are nuclear, or $\vec{\mu}_S = -\gamma_{\bar{e}}\hbar\vec{S}$, in case they are electronic. The factor γ is the gyromagnetic ratio of the particle under consideration, being, $\gamma_{\bar{e}} = 1.76 \times 10^{11}\frac{\text{rad}}{\text{s}\cdot\text{T}}$ (10) for a electron and $\gamma_{^{15}N} = -2.71 \times 10^{7}\frac{\text{rad}}{\text{s}\cdot\text{T}}$ (10) for a ^{15}N nuclei. In both cases, the spin operators are expressed in terms of the Pauli Matrices. Under a constant uniform magnetic field $\vec{B}_0 = B_0\hat{k}$, the system's Hamiltonian will be[1] (11)

$$\mathcal{H}_0 = -\vec{\mu}\cdot\vec{B}_0 = -\frac{\gamma\hbar B_0}{2}\sigma_z = -\frac{\hbar\omega_0}{2}\sigma_z, \tag{2.10}$$

where the defined quantity $\omega_0 \equiv \gamma B_0$ is denominated the Larmor frequency. This Hamiltonian has two eigenstates: $|-1/2\rangle$ and $|+1/2\rangle$, which can be simply associated into the computational basis: $|-1/2\rangle \to |1\rangle$ and $|+1/2\rangle \to |0\rangle$. Their eigenvalues are given by the Schrödinger Equation:

$$\mathcal{H}_0\,|\pm 1/2\rangle = -\frac{\hbar\omega_0}{2}\sigma_z\,|\pm 1/2\rangle = \mp\frac{\hbar\omega_0}{2}\,|\pm 1/2\rangle\,. \tag{2.11}$$

Thus, $E_0 = -\hbar\omega_0/2$ and $E_1 = \hbar\omega_0/2$. Using the σ_z basis, the thermal equilibrium density operator of the ensemble, given by Eq. (2.7), is written as

$$\rho_0 = \frac{e^{-\hbar\omega_0\sigma_z/2kT}}{\mathcal{Z}} = \frac{1}{\mathcal{Z}}\begin{bmatrix} e^{\hbar\omega_0/2kT} & 0 \\ 0 & e^{-\hbar\omega_0/2kT} \end{bmatrix}. \tag{2.12}$$

With the purpose of manipulating the quantum states, the spin ensemble can be

[1] In this convention, the sign becomes positive if the particle has negative charge, as an electron.

subjected to a short electromagnetic pulse in the perpendicular plane to the quantization z-axis. Such pulse of frequency Ω can be given by a rotating magnetic field in the xy-plane, expressed by $\vec{B}_1(t) = B_1\cos(\Omega t)\hat{i} + B_1\sin(\Omega t)\hat{j}$. The new Hamiltonian will have a contribution from both the static and rotating magnetic fields:

$$\mathcal{H}_1 = -\vec{\mu}\cdot(\vec{B}_0 + \vec{B}_1) = -\frac{\hbar\omega_0}{2}\sigma_z - \frac{\gamma\hbar}{2}\vec{B}_1(t)\cdot\vec{\sigma}. \tag{2.13}$$

Moreover, it is useful to adopt a rotating frame of reference, such that the rotating magnetic field remains static over one of the rotating axis $\hat{i}^{rot}$, hence $\vec{B_1}^{rot}(t) = B_1\hat{i}^{rot}$. In this frame, the pulse Hamiltonian from Eq. (2.13) is transformed accordingly with the proper rotation operator (11), resulting in the effective Hamiltonian of

$$\mathcal{H}_{eff} = e^{-i\Omega t\sigma_z/2}\,\mathcal{H}_1\,e^{i\Omega t\sigma_z/2} + \frac{\hbar\Omega}{2}\sigma_z = -\frac{\hbar}{2}(\omega_0 - \Omega)\sigma_z - \frac{\hbar\gamma B_1}{2}\sigma_x, \tag{2.14}$$

where σ_x is referent to the x-axis of the rotating frame. Adjusting the pulse frequency near the Larmor $\Omega \cong \omega_0$ results in

$$\mathcal{H}_{eff} \cong -\frac{\hbar\gamma B_1}{2}\sigma_x. \tag{2.15}$$

The effective Hamiltonian permits us to calculate the outcome of such pulse in the quantum states of the system. Prior to that, the density matrix from Eq. (2.12) must also be transformed to the rotating frame as

$$\rho_0^{rot} = e^{-i\Omega t\sigma_z/2}\,\rho_0\,e^{i\Omega t\sigma_z/2} = e^{-i\Omega t\sigma_z/2}e^{i\Omega t\sigma_z/2}\,\rho_0 = \rho_0. \tag{2.16}$$

Therefore, it remains constant with this change of reference frame, as the rotation operator commutes with ρ_0. Using Eq. (2.9), the result of the effective Hamiltonian will be

$$\rho^{rot}(t) = e^{i\gamma B_1 t\sigma_x/2}\,\rho_0^{rot}\,e^{-i\gamma B_1 t\sigma_x/2} = R_x(-\theta)\rho_0 R_x(\theta). \tag{2.17}$$

Here it becomes evident that this pulse on the Larmor Frequency $\Omega = \omega_0$ reproduces a rotation operator over the x-axis of the rotating frame $R_x(\theta) = e^{-i\theta\sigma_x/2}$, with a nutation angle $\theta = \gamma B_1 t_p$, where t_p is the pulse duration. This phenomenon is called magnetic resonance. Due to characteristics gyromagnetic ratios, the frequency required for the resonance varies largely with the particle, typically being in the range of radio frequencies for nuclear spins and microwaves for electrons. This is experimentally advantageous, given that it is possible to excite different spins species inside a sample without affecting others.

Analogously, the pulse could also have been taken on the y-axis of the rotating frame, thus generating a $R_y(\theta) = e^{-i\theta\sigma_y/2}$ rotation operator, or more generally, over any desired axis $\hat{n}$, $R_{\hat{n}}(\theta) = e^{-i\theta\hat{n}\cdot\vec{\sigma}/2}$. These rotation operators are expressed by an exponential power series and using the Pauli Matrices properties of: $\sigma_x^2 = \sigma_y^2 = \sigma_z^2 = \mathbb{1}$, they can be further simplified and written in matrix representation

$$R_x(\theta) = e^{-i\theta\sigma_x/2} = \cos(\theta/2)\mathbb{1} - i\,\sin(\theta/2)\sigma_x = \begin{bmatrix} \cos\left(\frac{\theta}{2}\right) & -i\,\sin\left(\frac{\theta}{2}\right) \\ -i\,\sin\left(\frac{\theta}{2}\right) & \cos\left(\frac{\theta}{2}\right) \end{bmatrix}, \tag{2.18}$$

$$R_y(\theta) = e^{-i\theta\sigma_y/2} = \cos(\theta/2)\mathbb{1} - i\,\sin(\theta/2)\sigma_y = \begin{bmatrix} \cos\left(\frac{\theta}{2}\right) & -\sin\left(\frac{\theta}{2}\right) \\ \sin\left(\frac{\theta}{2}\right) & \cos\left(\frac{\theta}{2}\right) \end{bmatrix} \text{ and} \tag{2.19}$$

$$R_z(\theta) = e^{-i\theta\sigma_z/2} = \cos(\theta/2)\mathbb{1} - i\,\sin(\theta/2)\sigma_z = \begin{bmatrix} \cos\left(\frac{\theta}{2}\right) - i\,\sin\left(\frac{\theta}{2}\right) & 0 \\ 0 & \cos\left(\frac{\theta}{2}\right) + i\,\sin\left(\frac{\theta}{2}\right) \end{bmatrix}. \tag{2.20}$$

By adjusting the duration of the pulse, it is possible to produce any angle of nutation, where the two most common rotations are with angles π and $\pi/2$, which are simply referred as $(\pi)_{\hat{n}}$-pulse and $(\pi/2)_{\hat{n}}$-pulse. Using these matrix representations, we can compute the effect of a rotation on the density operator. As an example, the $(\pi)_x$-pulse acts on the density operator from Eq. (2.12) accordingly as

$$\rho_\pi^{rot} = R_x(-\pi)\rho_0 R_x(\pi) = \frac{1}{\mathcal{Z}} \begin{bmatrix} e^{-\hbar\omega_0/2kT} & 0 \\ 0 & e^{\hbar\omega_0/2kT} \end{bmatrix}. \tag{2.21}$$

This result shows that a $(\pi)_x$-pulse inverts the populations from the initial thermal equilibrium. Similarly, the $(\pi/2)_x$-pulse acts as

$$\rho_{\pi/2}^{rot} = R_x\left(-\frac{\pi}{2}\right)\,\rho_0\,R_x\left(\frac{\pi}{2}\right) = \frac{1}{2}\begin{bmatrix} 1 & -i\,\tanh\left(\frac{\hbar\omega_0}{2kT}\right) \\ i\,\tanh\left(\frac{\hbar\omega_0}{2kT}\right) & 1 \end{bmatrix} = \frac{\mathbb{1}}{2} + \tanh\left(\frac{\hbar\omega_0}{2kT}\right)\frac{\sigma_y}{2}. \tag{2.22}$$

Thus, a $(\pi/2)_x$-pulse creates a perpendicular σ_y component on the density matrix.

The macroscopic effect of pulses are related to the expected value of the corresponding Pauli Matrices, given by Eq. (2.8). In the $(\pi)_x$-pulse, the macroscopic magnetization is simply inverted, while in the $(\pi/2)_x$-pulse there is the appearance of a transverse magnetization precessing around the static field (11). Magnetic resonance experiments typically measure these macroscopic manifestations by an indirect effect, like the induced electric current in a coil or by optical techniques, as is the case of the NV center. With the correct measurement of the macroscopic observable, it is possible to calculate the states populations of the qubits.

For QIP, the whole interest of generating spins rotations is to create quantum logic gates. As described so far, the perpendicular pulses produce rotations that can be represented by the matrices given in Eqs. (2.18), (2.19) and (2.20). In turn, these rotations form a basis of the 2×2 matrix space of all quantum gates acting on one qubit and thus can be used to compose a range of different gates. The Z gate from Eq. (2.2), for

instance, can be obtained with a $R_z(\pi)$ rotation:

$$R_z(\pi) = \begin{bmatrix} -i & 0 \\ 0 & i \end{bmatrix} = -i \begin{bmatrix} 1 & 0 \\ 0 & -1 \end{bmatrix} = e^{-i\pi/2} Z. \tag{2.23}$$

This shows that the Z gate and the $R_z(\pi)$ rotation are related through a $e^{-i\pi/2}$ phase, which is irrelevant to macroscopic measurements, as long as it can be turned into a global phase.

The Hadamard from Eq. (2.3), can be decomposed, apart from a phase, by a pulse sequence of a $(-\pi/2)_y$-pulse followed by a $(-\pi)_z$-pulse

$$R_z(-\pi)R_y(-\pi/2) = \frac{1}{\sqrt{2}} \begin{bmatrix} i & 0 \\ 0 & -i \end{bmatrix} \begin{bmatrix} 1 & 1 \\ -1 & 1 \end{bmatrix} = \frac{1}{\sqrt{2}} \begin{bmatrix} i & i \\ i & -i \end{bmatrix} = e^{i\pi/2} H. \tag{2.24}$$

In some practical applications, it is advantageous to suppress the $R_z(-\pi)$ rotation from the gate, resulting in the pseudo-Hadamard gate, given simply by

$$h \equiv R_y(-\pi/2) = \begin{bmatrix} 1 & 1 \\ -1 & 1 \end{bmatrix} \quad \text{and} \quad h^\dagger \equiv R_y(\pi/2) = \begin{bmatrix} 1 & -1 \\ 1 & 1 \end{bmatrix}. \tag{2.25}$$

3 Nitrogen Vacancy Centers as Quantum Processors

A pure diamond lattice is composed of carbon atoms arranged in a face-centered cubic structure. Defects in the lattice can occur naturally, where most commonly carbons get substituted by another atom or a vacancy, without altering the lattice structural geometry. The NV consists of one of such defects, where there is the substitution of a carbon for a nitrogen atom adjacent to a vacancy. A diamond sample doped with nitrogen-vacancies can contain a large number of centers, with densities up to 10^3 NV/μm^3 (6). An illustration of the NV can be seen in Fig. 1.

The quantization axis of the NV is defined as the one containing the vacancy and the nitrogen. Due to the face-centered cubic structure, the center has a 120^o rotation symmetry along the axis and can present four different orientations over the crystallographic axes. The four orientations are equally present in a sample and are labeled as: [111], [$1\bar{1}\bar{1}$], [$\bar{1}1\bar{1}$] and [$\bar{1}\bar{1}1$] (see Fig. 1).

An NV center can also exist at four different charge states (3): NV^{+1} NV^0, NV^{-1} and NV^{-2}. The NV^{-1} has six electrons, three from the surrounding carbons, two from the nitrogen valence shell and one captured from the bulk. Two of these electrons are unpaired and combined, result in a spin of either S=1 or S=0. The -1 charge state also has greater stability than the -2 and +1 states (3) and leads to an elaborate energy structure which can be exploited for QIP, unlike the 0 charge state. In sight of this, we focus the discussion exclusively in the NV^{-1}, which is simply referred as NV.

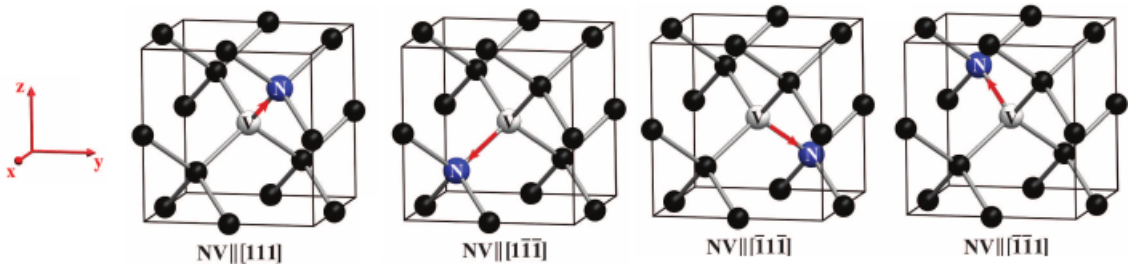

Figure 1: NV defect inside the face-centered cubic structure of diamonds.
The NV center is composed of a nitrogen substitution (blue) next to a vacancy (white) in the carbon lattice (black). The quantization axis can be in one of the four crystallographic orientations with equal probability.

Source: PHAM. *et al* [12]

From the perspective of QIP, there are four spin species present in an NV diamond. The electronic center (S=1 or S=0), the ^{15}N nuclei (I=1/2), the ^{14}N nuclei (I=1) and the ^{13}C nuclei (I=1/2), which unlike the ^{12}C, has a spin different from zero. The diamond considered in this study and used in our laboratory, presents almost exclusively the ^{15}N nitrogen isotope. With this, an NV diamond can constitute an ensemble of atomic scale quantum processors, each one with at least two qubits, the first represented by the spin resulting of the electronic center and the second the ^{15}N nuclear spin. The ^{13}C can also be used for QIP (4) and generates decoherence in the electronic spin states, however it has a more complicated mechanism of interaction with the other spins and thus it is not considered here.

Using the concepts introduced in section 2, in this section we characterize the NV center as a quantum processor and point out the important aspects and techniques for the realization of QIP. In 3.1, we study the energy structure of the center and the main interactions present in a simplified Hamiltonian. We present in 3.2 a viable optical magnetic mechanism for initializing and measuring the states, making use of the elaborate energy structure of the system. In 3.3, we analyze the application of electromagnetic pulses to generate quantum logic gates. Lastly, in 3.4, we point out the sources of decoherence in the NV diamond and the resulting coherence times of the states, limiting the overall duration of quantum algorithms and protocols.

3.1 Energy States and Hamiltonian

Section 2.3 discussed how a two energy level spin system can be used as computational space for QIP, in addition to describing the employment of magnetic resonance techniques for the application of quantum gates. However, the NV center does not exhibit only two energy levels, it has a rather more complex energy structure. Therefore, it is required a deeper look into the energy structure of both the electronic center and the ^{15}N nuclei, characterizing two energy states as the computational basis.

In a diamond, the sp^3 orbitals of the carbon atoms superpose, forming the valence and the conduction bands. This band-gap at room temperature has an energy difference of 5.47 eV (9), which corresponds to photons far more energetic than the visible spectrum, making a pure diamond transparent. On the other hand, the NV impurities create new energy states within the band gap, which makes the diamond acquire a yellowish colour. These inter band-gap states are suitable for QIP due to their spatially localized nature and some of the energy differences well above the thermal free energy kT, in this way, avoiding unwanted excitations.

As mentioned, the center electrons combine into S=1 or $S = 0$, corresponding to a triplet state and a singlet metastable state. Both configurations have excited and ground states within the band-gap. The triplet states are denominated respectively as ^{3}E and ^{3}A, while the singlets are ^{1}E and ^{1}A. The energy difference between the excited and ground state of the singlet is approximately 1.19 eV, while the energy between the lowest sublevel in ^{3}E and the highest in ^{3}A is 1.96 eV.

In order to better understand the NV center energy structure, it is necessary to analyze the system's Hamiltonian. In a simplified model (2 - 6), we only consider four main interactions: Zero-Field ($\mathcal{H}_{zf}$), Electron Zeeman ($\mathcal{H}_Z^{\bar{e}}$), Hyperfine Coupling between nuclei and electrons ($\mathcal{H}_{hf}$) and ^{15}N Nuclear Zeeman ($\mathcal{H}_Z^N$). With that

$$\mathcal{H} = \underbrace{\vec{S}^T \bar{D} \vec{S}}_{\mathcal{H}_{zf}} + \underbrace{\gamma_{\bar{e}} \vec{S} \cdot \vec{B}}_{\mathcal{H}_Z^{\bar{e}}} + \underbrace{\vec{S}^T \bar{A} \vec{I}}_{\mathcal{H}_{hf}} - \underbrace{\gamma_{^{15}N} \vec{I} \cdot \vec{B}}_{\mathcal{H}_Z^N}, \tag{3.1}$$

where $\bar{D}$ is the Zero-Field Tensor, $\bar{A}$ is the Hyperfine Tensor, $\vec{I}$ the nuclear spin operator (I=1/2) and $\vec{S}$ is the electronic spin operator of the center (S=1). The gyromagnetic ratios of the electron and the ^{15}N nuclei are given in section 2.3. Here, the ^{15}N nucleus does not present Electric Quadrupolar Interaction, different to what would have been the case with the ^{14}N isotope.

The most prominent of these interactions is the Zero-Field splitting in the triplet configuration, caused by the dipolar spin-spin interaction between the two unpaired electrons. It results in an energy difference between the $m_s = \pm 1$ and $m_s = 0$ states corresponding to 2.87 GHz in the ground state and 1.44 GHz in the excited state. Apart from that, there is a further Zeeman splitting of the electronic sublevels with $m_s = +1$ and $m_s = -1$. This energy difference depends on the external field and in units of frequency is given by $\Delta\nu = \Delta E/h = \gamma_{\bar{e}} B_{ext}/2\pi$, typically much smaller than the Zero-Field splitting, but still noticeable. Accounting for these two dominant interactions and neglecting the Hyperfine Coupling with the nitrogen nuclei, the energy states of the electronic spin are graphically represented in Fig. 2. Although the Nuclear Zeeman Interaction and the Hyperfine Coupling do not represent significant changes in the energy values of the electronic states,

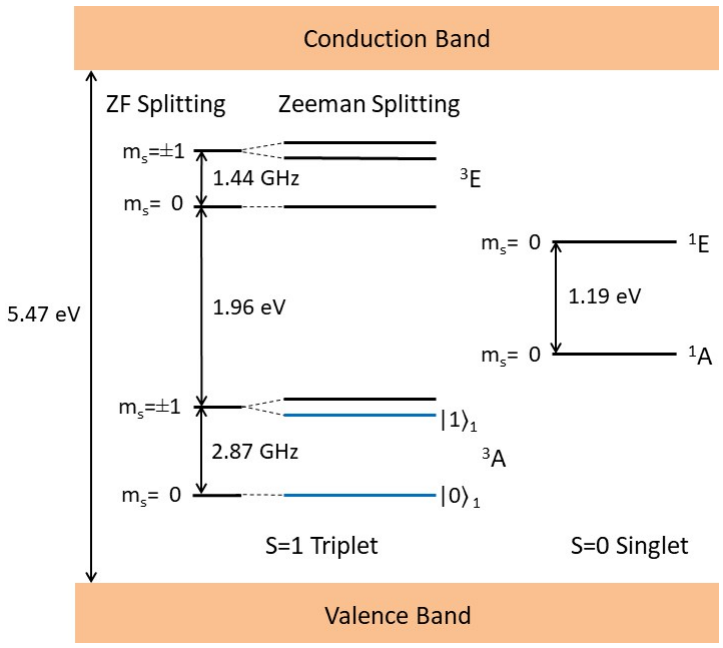

Figure 2: Diagram representation of the electronic energy level.
The center can be on a triplet configuration, with excited ^{3}E and ground ^{3}A states, or in a singlet configuration, with a excited ^{1}E and a ground ^{1}A state. The triplet suffers further splittings due to Zero-Field and Zeeman interactions. The energy differences between states are represented in different units, by virtue of distinct transition mechanisms. The two energy states used as the computational basis of the electronic qubit are labeled in blue.

Source: By the author.

they are of vital importance for QIP. The Hyperfine Coupling, for instance, is responsible for the interaction between both qubits.

At room temperature thermal equilibrium, the electronic spins mostly occupy the ^{3}A states equally, due to this energy difference being smaller than the thermal energy kT. Based on that and on the energy transition and excitation mechanisms that will be discussed in sections 3.2 and 3.3, the ground states with $m_s = 0$ and $m_s = -1$ are chosen as the computational states $|0\rangle_1$ and $|1\rangle_1$ for the electronic center qubit. For the second qubit, the association between the ^{15}N nuclear spin states and the computational basis is $|m_I = 1/2\rangle \rightarrow |0\rangle_2$ and $|m_I = -1/2\rangle \rightarrow |1\rangle_2$, however this association is not straightforward, as both states suffer a noticeable splitting due to the Hyperfine Coupling with the electronic spin.

Eq. (3.1) depends on the center orientation in respect to the external magnetic field. Thus, all four quantization axis orientations will result in different energy levels. For the purpose of proceeding with the system's characterization for QIP, we restrict the discussion to only one of the orientations. In principle, the external magnetic field can be adjusted parallel to one of them, such that $\vec{B}_0 = B_0\,\hat{k}$. In this case, the Zeeman interactions will only present parallel components to the quantization axis and, neglecting other perpendicular components from the Zero-Field and Hyperfine interactions, the

Hamiltonian can be further approximated to (6)

$$\mathcal{H} \cong D\left(S_z^2 - \frac{S^2}{3}\right) + \gamma_{\bar{e}} B_0 S_z - A_{zz} S_z I_z - \gamma_{^{15}N} B_0 I_z. \tag{3.2}$$

The values of these constants were experimentally measured at room temperature (2): $D = 2\pi \times 2.87$ GHz and $A_{zz} = 2\pi \times 3.03$ MHz [2]. It is important to emphasize that this is only valid for roughly one fourth of the centers and from now on, the study only concerns with centers with this particular orientation.

Having knowledge of the energy structure and a model for the Hamiltonian interactions is still not enough for characterizing the NV center as a QIP platform. A quantum computer needs a viable process of initialization, manipulation and reading of the quantum states. The next two sections will explore the energy structure in the interest of doing this characterization.

3.2 Initialization and Measurement of States

Prior to the application of any quantum algorithm or protocol, it is required to initialize the system in the desired computational state. A great advantage of the NV system is the presence of a simple optical pumping mechanism capable of doing so, in addition to providing a viable measurement method for the quantum states populations of the electronic centers.

The NV center can be optically excited in a spin conserving transition from the ^{3}A states to the ^{3}E states through the application of a green laser (532 nm). In the excited states, the center can lose energy to the surrounding lattice phonons and decay back to the ground states through the emission of photons. This decay process gives rise to a broad phonon sideband, ranging between 600 - 750 nm, but concentrated at the visible red. However, if there is no conversion of energy through phonon assisted vibrations, the emitted photons form a Zero-Phonon Line (ZPL) at 637 nm. The whole fluorescence spectrum is greatly affected by the temperature of the sample. With an increase in temperature, the phonon-assisted decay becomes increasingly predominant, thus making the ZPL less pronounced.

There is an alternative non-radiative relaxation path from the excited triplet. The electronic spins can suffer a non-spin-conserving decay to the excited singlet state ^{1}E, known as Intersystem Crossing. The spins then decay from the excited singlet state to the ground singlet state ^{1}A, emitting a photon of 1042 nm outside the fluorescence spectrum. Lastly, the spins decay back to the ground triplet. The excited states with $m_s = \pm 1$ are more likely to decay through this path, taking a much longer time ($\sim$300 ns (3)) compared to the $^3\text{E} \rightarrow {}^3\text{A}$ decay ($\sim$10 ns (3)). In addition to this, the ^{1}A state relaxes

[2] Some authors define both quantities without the 2π multiplicative term and a negative sign on A_{zz}.

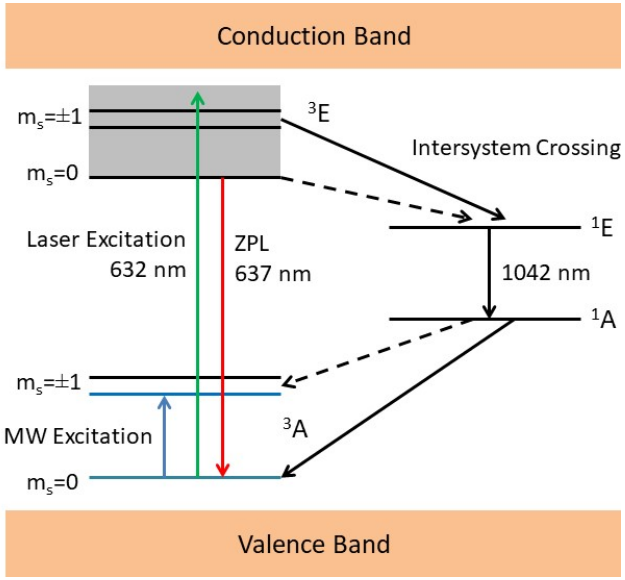

Figure 3: Diagram representation of the transitions between energy levels.
The green laser (green arrow) excite the ^{3}A states to the ^{3}E. A fluorescence spectrum is formed by the decay of these excited states with a characteristic ZPL (red arrow). The $m_s = \pm 1$ ^{3}E have a higher probability to decay through another non-spin-conserving path using the singlet states, which more likely decay back to $m_s = 0$ ^{3}A. Consequently, there is a pumping to the $|0\rangle_1$ state and their populations can be inferred by the fluorescence intensity. The microwave driving between $|0\rangle_1 \rightarrow |1\rangle_1$ is represented by the blue arrow.

Source: By the author.

with more probability to the $m_s = 0$ sublevel of the ground state than to the $m_s = \pm 1$. Therefore, after a few cycles there is an optical pumping to the $m_s = 0$ ^{3}A state and the ensemble is initialized in the $|0\rangle_1$ computational state. The optical excitation and both decay paths are graphically represented in Fig. 3.

Apart from enabling initialization, this optical excitation and decay mechanism of the NV center can be used to indirectly measure the quantum states populations. As the $m_s = \pm 1$ states decay more likely through the Intersystem Crossing than the $m_s = 0$, an increase in their populations leads to a decrease in the fluorescence intensity. Thereby, the measurement of this decrease in the photoluminescence results in a value directly proportional to the $|1\rangle_1$ ($m_s = -1$) state population. This technique is known as Optically Detected Magnetic Resonance (ODMR) and is largely used in magnetometry applications with the NV center (7).

The ODMR measurement method, in principle, does not require a large number of centers to produce a noticeable signal, as is the case in nuclear magnetic resonance. It is possible to account for even a single center in state of the art applications (4 - 5). In those cases, the ensemble formalism introduced in section 2.2 is not entirely valid. Also, compared to nuclear magnetic resonance, the initialization to a pure state can be done with relative ease, without the need to apply a pulse sequence for the preparation of a pseudo-pure state (13).

The nuclear states do not present a simple optical technique to initialize and measure their populations. Nevertheless, their states populations can be evaluated by indirect measurements of the electronic states using engineered protocols, as the one that will be presented in section 4.

3.3 Implementation of Quantum Logic Gates

It was shown in section 2.3 that pulses at the resonant frequency lead to rotations, which in turn can be used to create quantum logic gates. In the case of the electronic spin of the NV, the excitation between the ground triplet sublevels ^{3}A can be achieved with microwave pulses.

Under the application of an electromagnetic pulse, as in Eq. (2.12), and disregarding the weaker Hyperfine Coupling, the Hamiltonian of the electronic spin at the ^{3}A states will be

$$\mathcal{H}^{\bar{e}} \cong D\left(S_z^2 - \frac{S^2}{3}\right) + \gamma_{\bar{e}} B_0 S_z + \gamma_{\bar{e}} B_1 \left[S_x \cos(\Omega_{MW} t) + S_y \sin(\Omega_{MW} t)\right]. \tag{3.3}$$

Since $S^2 \propto \mathbb{1}$, it represents a uniform background, which can be neglected in time evolution calculations. With this, the effective Hamiltonian in the rotating frame of reference, analogous to Eq. (2.14), is represented in the S_z basis as

$$\mathcal{H}^{\bar{e}}_{eff} \cong DS_z^2 + \gamma_{\bar{e}} B_0 S_z + \gamma_{\bar{e}} B_1 S_x + \Omega_{MW} S_z = \begin{bmatrix} D + \gamma_{\bar{e}} B_0 + \Omega_{MW} & \frac{\gamma_{\bar{e}} B_1}{\sqrt{2}} & 0 \\ \frac{\gamma_{\bar{e}} B_1}{\sqrt{2}} & 0 & \frac{\gamma_{\bar{e}} B_1}{\sqrt{2}} \\ 0 & \frac{\gamma_{\bar{e}} B_1}{\sqrt{2}} & D - \gamma_{\bar{e}} B_0 - \Omega_{MW} \end{bmatrix}. \tag{3.4}$$

The resonant conditions are given when one of the main diagonal entries is null: $D \pm \gamma_{\bar{e}} B_0 \pm \Omega_{MW} = 0$. Thus, there are two resonance frequencies, one leading to the $|m_s = 0\rangle \rightarrow |m_s = +1\rangle$ transition and the other to the $|m_s = 0\rangle \rightarrow |m_s = -1\rangle$ transition inside the ^{3}A states. The relevant excitation for this work is between the computational basis states, $|0\rangle_1$ ($m_s = 0$) and $|1\rangle_1$ ($m_s = -1$), which corresponds to a resonant frequency deviated from the Larmor Frequency $\omega_0^{\bar{e}} \cong D - \gamma_{\bar{e}} B_0$. This excitation is represented in Fig. 3.

In an ODMR scan, the pulse frequency is swapped within a range and the resultant fluorescence is measured, indicating resonances, as discussed in section 3.2. The resonant frequency values obtained from Eq. (3.4) only apply to the parallel orientation of the quantization axis. Thereby, a scan of the NV center around the microwave band would result in a spectrum with eight distinct peaks (6 - 7). Each one of the four orientations of the quantization axis leading to the two peaks of each transition. The resonant frequency corresponding to the transition between the computational basis can be evaluated from such ODMR spectra.

By initializing the system in the $|0\rangle_1$ ($m_s = 0$) state and with the correct microwave

excitation to the $|1\rangle_1$ ($m_s = -1$) state, we can consider the electronic spin as a two energy level system, fitting the formalism of section 2. And thus, based on microwave pulse rotations, compose a range of different quantum logic gates, like the Z gate given by Eq. (2.23) or the Hadamard gate from Eq. (2.24). However, many experimental setups do not favour pulses in the z-axis. In such cases, the $R_z(\theta)$ rotation operator can be decomposed in three perpendicular pulses

$$R_z(\theta) = R_y(-\pi/2)R_x(\theta)R_y(\pi/2). \tag{3.5}$$

The other qubit, composed of the ^{15}N nuclear spin, has a more complex excitation mechanism. In this case, the Hyperfine Coupling is at the same order of magnitude as the Zeeman Interaction and cannot be neglected. Under a perpendicular radio frequency pulse,

$$\mathcal{H}^{^{15}N} = -A_{zz}S_zI_z - \gamma_{^{15}N}B_0I_z - \gamma_{^{15}N}B_1\left[I_x\cos(\Omega_{RF}t) + I_y\sin(\Omega_{RF}t)\right]. \tag{3.6}$$

The corresponding effective Hamiltonian in the rotating frame will then be

$$\mathcal{H}_{eff}^{^{15}N} = (\Omega_{RF} - A_{zz}m_s - \gamma_{^{15}N}B_0)I_z - \gamma_{^{15}N}B_1I_x. \tag{3.7}$$

From this equation, the resonant frequencies of the nuclei are $\omega_0^{^{15}N} = \gamma_{^{15}N}B_0 + A_{zz}m_s$, with $m_s = -1, 0, 1$. Therefore, the electronic state must be taken into account in the computation of the resonant frequency, which complicates the experimental excitation between the nuclear states. For that reason, some applications avoid nuclear states manipulations.

Apart from affecting the nuclear states, the Hyperfine Coupling is also essential to create controlled gates with the two qubits, as it governs the interaction between them. In the rotating frame, the Zero-Field and electronic Zeeman interactions can be compensated by the rotation at the resonant frequency. Disregarding the weaker Nuclear Zeeman Interaction, a free-evolution will be dominated by the Hyperfine Coupling and in these conditions is represented by the operator

$$U_f(t) = e^{-i\mathcal{H}_{hf}t} = e^{itA_{zz}I_zS_z}. \tag{3.8}$$

Applying it on an element of the electronic spins subspace results in $e^{itA_{zz}I_zS_z}|m_s\rangle = e^{itA_{zz}I_zm_s}|m_s\rangle$. Furthermore, if the electronic spin is in the state $|0\rangle_1$, then $m_s = 0$. Inversely, if the state is $|1\rangle_1$, then $m_s = -1$. The state $m_s = 1$ is not represented in the computational basis and, ideally, the system is initialized with population zero in this state, which again justifies neglecting it in this free-evolution and treating the problem in the 2-dimensional Hilbert space. With this, we can rewrite the free-evolution operator as

$$U_f(\tau) = |0\rangle\langle 0|_1 \otimes (e^0)_2 + |1\rangle\langle 1|_1 \otimes (e^{-i\tau A_{zz}I_z})_2 = |0\rangle\langle 0|_1 \otimes \mathbb{1}_2 + |1\rangle\langle 1|_1 \otimes R_z^{^{15}N}(A_{zz}\tau), \tag{3.9}$$

where the rotation operator is equivalent to in Eq. (2.20), but with a nutation angle of $\theta = A_{zz}\tau$.

By adjusting the free-evolution interval and composing it with other pulses, it is

possible to produce several distinct controlled gates. As an example, taking the interval as $\tau = \pi/A_{zz} \cong 165$ ns, results in the rotation $R_z^{^{15}N}(\pi) = e^{-i\pi/2}Z_2$. To create the $CtrZ$ gate from Eq. (2.5), it is necessary to make this phase global. To do so, we apply a $(\pi/2)_z$-pulse to the electronic spin:

$$R_z^{\bar{e}}\left(\frac{\pi}{2}\right) U_f \left(\frac{\pi}{A_{zz}}\right) = R_z^{\bar{e}}\left(\frac{\pi}{2}\right) |0\rangle \langle 0|_1 \otimes \mathbb{1}_2 + R_z^{\bar{e}}\left(\frac{\pi}{2}\right) |1\rangle \langle 1|_1 \otimes e^{-i\pi/2} Z_2. \tag{3.10}$$

Considering the relation between the computational basis and the spin basis, the rotation operator with S=1 acts on the computational basis as $R_z^{\bar{e}}(\pi/2)\,|0\rangle_1 = |0\rangle_1$ and $R_z^{\bar{e}}(\pi/2)\,|1\rangle_1 = i\,|1\rangle_1 = e^{i\pi/2}\,|1\rangle_1$. With this, Eq. (3.10) results in the CtrZ gate

$$R_z^{\bar{e}}\left(\frac{\pi}{2}\right) U_f \left(\frac{\pi}{A_{zz}}\right) = |0\rangle \langle 0|_1 \otimes \mathbb{1}_2 + e^{i\pi/2} e^{-i\pi/2} |1\rangle \langle 1|_1 \otimes Z_2 = CtrZ. \tag{3.11}$$

3.4 Decoherences of States

Decoherences of quantum states is a major issue for practical realizations of quantum computing. It can be understood as the loss of information of the system to the environment, or in the density matrix formalism, is represented by the decay and undesired alterations in the off-diagonal elements. This decoherence happens in a characteristic timescale of each system. In the NV center, the electronic spin suffers from two distinct mechanisms of decoherence, the longitudinal relaxation (T_1) and the transverse relaxations (T_2^* and T_2).

The longitudinal relaxation happens due to the spin-lattice interaction, leading to the establishment of thermal equilibrium with the external magnetic field and the exponential decay of the perpendicular magnetization. The rigid lattice of diamonds shields the center from many phonon assisted perturbations, leading to a long T_1 between 1 - 10 ms (6), depending on the temperature.

As for the transverse relaxation, it leads to spin dephasings in the perpendicular plane to the external field, happening faster than T_1. It can be decomposed into two components, a homogeneous spin dephasing T_2 and an inhomogeneous one, such that T_2^* is the resulting combination of both (14). The homogeneous component is due to the stochastic interaction between the electronic spin and vicinal nuclear spins. Due to its random and non-static nature, it is irreversible and characteristic of each NV diamond sample. Specifically designed NV diamonds for QIP, with a low concentration of centers, present T_2 timescale near T_1, however, the sample used in our laboratory has $T_2 \cong 2.17$ μs (6).

The inhomogeneous spin dephasing occurs due to inhomogeneities in the external magnetic field and other static local magnetic susceptibility variations between spins. These effects are static and can be reversed with proper echo pulses (6 - 11), resulting

in $T_2^* \cong T_2$. Alternatively, T_2^* can also be enhanced by focusing the initialization and measurement laser (section 3.2) in a smaller area (in the order of μm^2), thus with smaller inhomogeneities.

These timescales limit the overall duration of quantum algorithms and protocols, where the interval between initialization, pulse sequence and reading cannot extend beyond a point where great part of the qubits have lost coherence. It is clear that $T_1 > T_2 > T_2^*$, meaning that T_2^* is the most limiting timescale. However, as mentioned, with the proper techniques T_2^* can be taken to values near T_2, which in turn can be near T_1 of milliseconds in some samples. Being more than enough for the application of most quantum algorithms and protocols, even at room temperature.

4 A Non-Thermalizing Quantum Thermometer

In this section, we examine a quantum protocol capable of measuring the NV diamond temperature, illustrating the concepts and techniques discussed so far. A similar protocol was originally designed and executed in liquid chloroform molecules using nuclear magnetic resonance by Raitz *et al.* (13). Here, we adapt the protocol for the NV diamond, where the ensemble of electronic spins are used as probe qubits to measure the temperature of the target qubits, represented by the ^{15}N nuclear spins. Unlike a classical thermometer, the temperature is indirectly measured by the quantum properties of the system.

Thermometry with the NV diamond has already been widely studied and tested (15 - 16), paving the way for a potential thermometer with nanoscale spatial resolution, capable of measuring with high precision the temperature of nano structures in biological systems, semi-conductors or polymers. Differently from previous ones, this application is done entirely in a quantum protocol and brings an interesting concept of a non-thermalizing thermometer. This apparent violation of the 0^{th} Law of Thermodynamics (13), which states the establishment of thermal equilibrium between system and thermometer, resides in the fact that during the measurement, the probe qubits are not in thermal equilibrium with the target qubits. In this way, the whole protocol happens much faster than the relaxation times responsible for establishing thermal equilibrium, meaning that there is no thermalization between the probe and target qubits.

We begin in section 4.1 with an examination of the protocol, under the perspective of quantum information theory. In 4.2, we propose a pulse sequence to reproduce it using the NV system and discuss the expected results and possible difficulties in its experimental realization.

4.1 The Quantum Protocol

The protocol uses two qubits, the probe (electronic center spin) and the target (^{15}N nuclei spin), which we want to measure the temperature. This approach is also called a Quantum Scattering Circuit (13), due to the similarities of such experiments, where the variation in moment of a particle is known by measuring the variation in moment of the other colliding particle. The protocol is graphically represented by the quantum circuit in Fig. 4.

Prior to the manipulation of the qubits, the system must be prepared in an initial state with the probe in the $|0\rangle_1$ state and the target in thermal equilibrium at temperature T given by the 2×2 density matrix ρ, in the same conditions as in section 2. The density operator of the two qubit system is given by a 4×4 matrix resulting from the tensor product between the probe and target density operators:

$$\Psi_0 = |0\rangle \langle 0|_1 \otimes \rho_2 \equiv \begin{bmatrix} \rho & \mathbb{0} \\ \mathbb{0} & \mathbb{0} \end{bmatrix}, \tag{4.1}$$

where $\mathbb{0}$ is the 2×2 matrix with all elements null.

As an assumption, the manipulation of qubits is done fast enough that ρ does not evolve significantly. That being said, the first quantum gate is a Hadamard in the probe qubit, given by Eq. (2.4). This results in the density operator of

$$\Psi_1 = (H_1 \otimes \mathbb{1}_2)\, \Psi_0\, (H_1 \otimes \mathbb{1}_2)^\dagger = \frac{1}{2} \begin{bmatrix} \mathbb{1} & \mathbb{1} \\ \mathbb{1} & -\mathbb{1} \end{bmatrix} \begin{bmatrix} \rho & \mathbb{0} \\ \mathbb{0} & \mathbb{0} \end{bmatrix} \begin{bmatrix} \mathbb{1} & \mathbb{1} \\ \mathbb{1} & -\mathbb{1} \end{bmatrix}^\dagger = \frac{1}{2} \begin{bmatrix} \rho & \rho \\ \rho & \rho \end{bmatrix}. \tag{4.2}$$

Note that $H_1 \otimes \mathbb{1}_2$ is Hermitian. After that, the target qubit goes through a $CtrZ$ gate defined in Eq. (2.5), resulting in

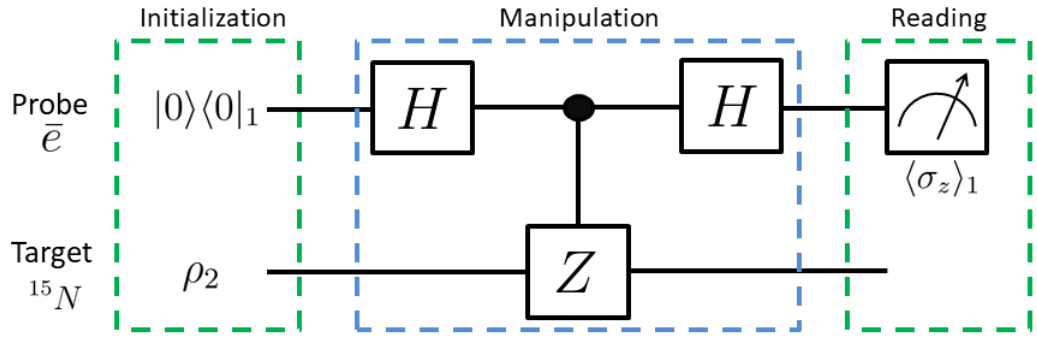

Figure 4: Quantum circuit representation of the protocol.
Initially the probe is in the state $|0\rangle_1$, while the target is in thermal equilibrium with temperature T given by the density matrix ρ. The probe goes through a Hadamard gate, the target qubits goes trough a Controlled Z gate, a Hadamard is applied again in the probe and finally $\langle\sigma_z\rangle_1$ is measured, wielding a result that depends on the target temperature.

Source: By the author.

$$\Psi_2 = (CtrZ)\,\Psi_1\,(CtrZ)^\dagger = \frac{1}{2}\begin{bmatrix}\mathbb{1} & \mathbb{0}\\ \mathbb{0} & Z\end{bmatrix}\begin{bmatrix}\rho & \rho\\ \rho & \rho\end{bmatrix}\begin{bmatrix}\mathbb{1} & \mathbb{0}\\ \mathbb{0} & Z\end{bmatrix}^\dagger = \frac{1}{2}\begin{bmatrix}\rho & \rho Z\\ Z\rho & Z\rho Z\end{bmatrix}. \tag{4.3}$$

The $CtrZ$ gate is also Hermitian. The third gate is once again a Hadamard in the probe qubit,

$$\Psi_3 = (H_1 \otimes \mathbb{1}_2)\,\Psi_2\,(H_1 \otimes \mathbb{1}_2)^\dagger = \frac{1}{4}\begin{bmatrix}\rho + Z\rho Z + (Z\rho + \rho Z) & \rho - Z\rho Z + (Z\rho - \rho Z)\\ \rho - Z\rho Z - (Z\rho - \rho Z) & \rho + Z\rho Z - (Z\rho + \rho Z)\end{bmatrix}. \tag{4.4}$$

Considering that $Z\rho Z = \rho$ and $Z\rho = \rho Z$, this final is represented by

$$\Psi_3 = \frac{1}{2}\begin{bmatrix}\rho + \rho Z & 0\\ 0 & \rho - \rho Z\end{bmatrix}. \tag{4.5}$$

This whole manipulation can be seen as a projection of the initial thermal equilibrium states of the target qubit into the probe qubit, happening before thermalization is reached between both. Hence, the probe qubit acquires information about the temperature of the target qubit without being in thermal equilibrium with it, justifying to denominate it a non-thermalizing thermometer.

In the objective to obtain information about the target qubits temperature, we can measure the expectation value of $\langle\sigma_z\rangle_1$ in the probe qubit. Using Eq. (2.8), it corresponds to

$$\langle\sigma_z\rangle_1 = \mathrm{Tr}\left\{\Psi_3[(\sigma_z)_1 \otimes \mathbb{1}_2]\right\} = \mathrm{Tr}\left(\frac{1}{2}\begin{bmatrix}\rho + \rho Z & 0\\ 0 & -\rho + \rho Z\end{bmatrix}\right) = \mathrm{Tr}[(\sigma_z)_2\,\rho], \tag{4.6}$$

where $Z = (\sigma_z)_2$ was used, due to the fact that both have the same matrix representation. Also, for clarification, $(\sigma_z)_1$ acts on the probe space and $(\sigma_z)_2$ on the target space. For a Hamiltonian $\mathcal{H}_0$, where the previous thermal equilibrium of the target qubits was established, the density operator ρ can be further substitute by Eq. (2.7), giving

$$\langle\sigma_z\rangle_1 = \mathrm{Tr}\left[\frac{(\sigma_z)_2\, e^{-\mathcal{H}_0/kT}}{\sum_j e^{-E_j/kT}}\right]. \tag{4.7}$$

The whole protocol enables that a measurement of $\langle\sigma_z\rangle_1$ in the probe qubits will result in a value dependent on the temperature of the target qubits. Therefore, by measuring some quantity proportional to $\langle\sigma_z\rangle_1$ and knowing the Hamiltonian $\mathcal{H}_0$ with its energy levels, it is possible to calculate the temperature. The following section focus on this issue with the NV center.

4.2 Proposal of Application with the NV System

Reproducing the protocol in a physical quantum processor is not straightforward. However, we have already discussed in sections 2 and 3 how the NV center can be used as a two qubit quantum processor, with feasible mechanisms of initialization, manipulation

and reading of states.

Primarily, the initialization to state $|0\rangle_1$ of the probe qubit can be accomplished with the optical pumping described in section 3.2. The quantum gates of the protocol can then be produced by microwave pulses with the proper resonant frequency correspondent to the $|m_s = 0\rangle \rightarrow |m_s = -1\rangle$ transition of the electronic spin, as we have shown in 3.3. In this case, without affecting the result, the first Hadamard gates can be substituted by a Pseudo-Hadamard Gate and the second by its conjugate, both given in Eq. (2.25).

The Controlled Z gate from Eq. (3.11) is achieved by a free evolution of $\tau = \pi/A_{zz}$, followed by the application of a $(\pi/2)_z$-pulse on the electronic qubit. However, in this case the z-pulse must be decomposed by perpendicular pulses, as in Eq. (3.5). With this, the whole pulse sequence that gives rise to the protocol is

$$\begin{aligned} h_1^\dagger \, Ctr Z \, h_1 &= \left[R_y^{\bar{e}}\left(\frac{\pi}{2}\right)\right]\left[R_y^{\bar{e}}\left(-\frac{\pi}{2}\right) R_x^{\bar{e}}\left(\frac{\pi}{2}\right) R_y^{\bar{e}}\left(\frac{\pi}{2}\right) U_f \left(\frac{\pi}{A_{zz}}\right)\right]\left[R_y^{\bar{e}}\left(-\frac{\pi}{2}\right)\right] \\ &= R_x^{\bar{e}}\left(\frac{\pi}{2}\right) R_y^{\bar{e}}\left(\frac{\pi}{2}\right) U_f \left(\frac{\pi}{A_{zz}}\right) R_y^{\bar{e}}\left(-\frac{\pi}{2}\right). \end{aligned} \tag{4.8}$$

As we have shown in section 3.3, the corresponding time of the free evolution is $\tau \cong 165$ ns. Also, in order to avoid additional decoherences, the pulse amplitude B_1 must be adjusted to a high power, thus taking the pulse duration to a minimum. In the setup used in our laboratory, the pulse duration can achieve a value as low as 10 ns to 20 ns. Adding all the duration of the pulses and the free-evolution, the total duration of the protocol stands above 200 ns, which is at the same order of magnitude of the inhomogeneous spin dephasing T_2^* of several hundred nanoseconds. That being said, the fidelity of measurement could be compromised, making necessary the incorporation of special techniques to maintain the states coherence, as mentioned in 3.4. A solution to this issue is currently in development in our laboratory.

Lastly, the observable $\langle\sigma_z\rangle_1$ of Eq. (4.7) can be measured by the fluorescence intensity of the sample. As described in section 3.2, an increase in the $m_s = -1$ state population, and consequently $\langle\sigma_z\rangle_1$, results in a decrease of the fluorescence. With this, the decrease in the photoluminescence is expected to be linearly proportional to $\langle\sigma_z\rangle_1$, with two coefficients to be calculated by calibration. The resulting measurement will not only depend on the temperature of the ^{15}N nuclear spins ensemble, but also on the Hamiltonian $\mathcal{H}_0$, upon which their thermal equilibrium was established prior to the pulse sequence. In this thermal equilibrium, the electronic qubits were all initialized in the state with $m_s = 0$, causing the Hyperfine Coupling to be null. Thus, the Hamiltonian $\mathcal{H}_0$ only

depends on the Nuclear Zeeman Interaction, $\mathcal{H}_Z^N$ from Eq. (3.1),

$$\langle\sigma_z\rangle_1 = \mathrm{Tr}\left\{\frac{(\sigma_z)_2\, e^{\hbar\omega_0^N(\sigma_z)_2/2kT}}{\mathcal{Z}}\right\} = \frac{1}{2}\mathrm{Tr}\left[(\sigma_z)_2 + \tanh\left(\frac{\hbar\omega_0^N}{2kT}\right)\mathbb{1}\right] = \tanh\left(\frac{\hbar\omega_0^N}{2kT}\right), \tag{4.9}$$

due to the fact that ${(\sigma_z)_2}^2 = \mathbb{1}$, $\mathrm{Tr}[(\sigma_z)_2] = 0$ and $\mathrm{Tr}(\mathbb{1}) = 2$. Based on this result, the thermometer must be calibrated with known temperatures, just as most thermometers, so that the two coefficients of the relation between the measured fluorescence intensity and $\tanh\left(\hbar\omega_0^N/2kT\right)$ can be evaluated.

This protocol has never been applied to the NV center. For this reason, there are many experimental difficulties or possible corrections to the model that are not yet clear and are under development in our laboratory. Besides the decoherence times, the main sources of errors are related to the optical measurement of the fluorescence and the calibration of pulses, as any nanosecond of error in its duration would represent a substantial relative deviation of the desired nutation angle. The low amplitude of the measured decrease in the fluorescence intensity is another limiting experimental issue. Furthermore, neglecting the perpendicular terms in Eq. (3.2) or the assumption that the initial density matrix ρ does not evolve significantly during the pulse sequence remain to be tested and, possibly, corrected in the experiments.

Conclusion and Outlook

In this study we examined how the NV diamond can be used as a platform for the physical realization of QIP. The system configures a quantum computer composed of an ensemble of atomic scale quantum processors realizing parallel computing, with each of the centers having at least two qubits. The first qubit is represented by the spin resulting from the combination of the center electrons, with S=1. While the second is represented by the ^{15}N nuclear spin with I=1/2. The NV center with charge state -1 has an elaborate energy structure within the band gap, where the basis states of the electronic qubit were associated as $m_s = 0 \rightarrow |0\rangle_1$ and $m_s = -1 \rightarrow |1\rangle_1$ sublevels of the ground state triplet ^{3}A.

The energy structure of the NV center permits the electronic qubit to be initialized in the $|0\rangle_1$ state by optical pumping. Using the same optical decay, the electronic qubit populations can be indirectly evaluated by the measurement of the fluorescence intensity. Furthermore, the excitation $|0\rangle_1 \rightarrow |1\rangle_1$ is accomplished with the incidence of microwave pulses. With the right pulse sequence, a vast number of quantum logic gates can be performed. These simple mechanisms of initialization, manipulation and reading of the quantum states make the NV system a viable platform for QIP even at room temperature.

To exemplify the discussed concepts, we adapted to the NV diamond a protocol

for measuring the temperature of a spin ensemble. In the protocol, the electronic spins interact with the ^{15}N nuclear spins and are used to indirectly measure their ensemble temperature. The measurement is made prior to the thermal equilibrium between the probe and the target being reached, making it a non-thermalizing thermometer. The research can now focus on the experimental realization of the protocol and its inherent complications, namely the loss of coherence, the application of microwave pulses and the amplitude of the measured signal. The spin dephasing timescale T_2^* has proven to be at the same order of magnitude as the pulse sequence duration, which can represent a challenge to the implementation. This effort is currently being pursued in our laboratory.

References

1 ARUTE, F. *et al.* Quantum supremacy using a programmable superconducting processor.*Nature* ,v.574, p.505-510,2019. DOI:10.1038/s41586-019-1666-5.

2 WU, Y. *et al.* A programmable two-qubit solid-state quantum processor under ambient conditions. NPJ Quantum Information, v.5, n.9, 2019. DOI:10.1038/s41534-019-0129-2.21

3 WEBER,J. R. *et al.* Quantum computing with defects. *Proceedings of the National 'Academy of Sciences*, v.107, n.19, p.8499-8518, 2010. DOI:10.1073/pnas.1003052107.

4 JELEZKO, F. *et al.* Observation of coherent oscillation of a single nuclear spin and realization of a two-qubit conditional quantum gate. *Physical Review Letters*, v.93,2004. DOI:10.1103/PhysRevLett.93.130501.

5 GURUDEV, M. V. *et al.* Quantum register based on individual electronic and nuclear spin qubits in diamond. *Science*, v.316, p.1312-1316, 2007. DOI:10.1126/science.1139831.

6 SEGURA, C. *Diamond studies for applications in quantum technologies.* 2019. (Doctoral Thesis) - Instituto de Fisica de Sao Carlos, Universidade de Sao Paulo, Sao Carlos, 2019.

7 ACOSTA, M. *Optical magnetometry with nitrogen-vacancy centers in diamond.* (Doctoral Thesis) - University of California, Berkeley, California, 2011

8 COHEN-TANNOUDJII, C.; DIU,B.; LALOE,F. *Quantum mechanics.* New York: Wiley Pvt.Limited, 1991. v.1.

9 KITTEL, Charles. *Introduction to solid state physics.*7th ed. New York: Wiley Pvt.Limited, 2007.

10 NIST: National Institute of Standards and Technology, Available on: https://physics.nist.gov/cgi-bin/cuu/Value?gammae. Acessible at: 16 April, 2020.

11 SLICHTER, C. P. *Principles of magnetic resonance.* 3rd. ed. Berlin: Springer-Verlag,1990.

12 PHAM, L. M. *et al.* Enhanced metrology using preferential orientation of nitrogen-vacancy centers in diamond. *Physical Review*, v.86, n.12, 2012. DOI:10.1103/PhysRev B.86.121202.

13 RAITZ, C. *et al.* Experimental implementation of a nonthermalizing quantum thermometer.*Quantum Information Process*, v.14, p.37{46, 2015. DOI:10.1007/s11128-014-0858-z.

14 JUNG, B.A. *et al.* Spin echo magnetic resonance imaging. *Journal of Magnetic Resonance Imaging*, v.37, p.805-817, 2013. DOI:10.1002/jmri.24068.

15 NEUMANN, P. *et al.* High-precision nanoscale temperature sensing using single defects in diamond. *Nano Letters*, v.13, n.6, p.2738-2742, 2013. DOI:10.1021/nl401216y.

16 TOYLI, D. *et al.* Fluorescence thermometry enhanced by the quantum coherence of single spins in diamond. *Proceedings of the National Academy of Sciences*,v.110, n.21, p.8417-8421, 2013. DOI:10.1073/pnas.1306825110.